UNITED NATIONS EDUCATIONAL, SCIENTIFIC AND CULTURAL ORGANIZATION
INTERNATIONAL ATOMIC ENERGY AGENCY
INTERNATIONAL CENTRE FOR THEORETICAL PHYSICS
I.C.T.P., P.O. BOX 586, 34100 TRIESTE, ITALY, CABLE: CENTRATOM TRIESTE

SMR.998b - 4

Research Workshop on Condensed Matter Physics
30 June - 22 August 1997
MINIWORKSHOP ON
SUPERCONDUCTING MESOSCOPIC STRUCTURES

14 - 25 JULY 1997

"Andreev reflection spectroscopy in point contacts" (A Review)

I.K. YANSON
Academy of Sciences of Ukraine
Institute for Low Temperature Physics & Engineering
Department of Theoretical Physics
47 Lenin Av.
310164 Kharkov
UKRAINE

Andreev reflection spectroscopy in point contacts (A Review)

I.K. Yanson
Institute for Low Temperature Physics and Engineering, 310164 Kharkiv, Ukraine
(June 6, 1997)

In experiments with 3D point contacts (PC) often very little is known *apriori* about the contact geometry, chemical and physical structure, electron and phonon mean free paths, *etc.* This hinders correct interpretation of contact properties. In introduction we describe various techniques for preparations of 3D contacts and apply the normal-state inelastic PC spectroscopy [1,5] for their characterization.

The Andreev-reflection spectroscopy of point contacts makes use of energy dependence of excess current which appears due to specific reflection of quasiparticle from $N-S$ boundary. The magnitude of excess current depends on the contact purity. We show how to determine the ratio of l_e, the elastic electron mean free path, and d, the contact size, from the intensity of normal-state electron-phonon interaction (EPI) PC spectra, and argue that $l_e/d \leq 0.5$ is enough to make the contact dirty.

The excess current at large voltages ($eV > \Delta$) is not constant. It has small nonlinearities due to EPI. For clean contacts, most important are inelastic processes and strong-coupling EPI effects involved in Andreev-reflection processes. Inelastic processes with emission of real phonons occur when electron quasiparticle with energy of the order of eV relaxes to the hole state appearing due to Andreev reflection of another electron with energy of the order of Δ. This leads to the correction to excess current of the order of $I^{(0)}_{exc}(d/l_i)$, where $I^{(0)}_{exc} \sim \Delta/R$ (R is the contact resistance and l_i inelastic mean free path) [16]. The strong coupling electron-phonon effects correspond to energy dependence of complex superconducting order parameter $\Delta(E)$ and lead to correction of the order of $I^{(0)}_{exc}[\Delta(E)/\hbar\omega_{ph}]$ [17]. This is an analogy to $[\Delta(E)/\hbar\omega_{ph}]^2$ correction to the total contact current in the Rowell-McMillan-Dynes tunneling spectroscopy of superconductors with characteristic phonon energies $\hbar\omega_{ph}$. We present experimental evidence confirming these results.

In dirty contacts the situation is vague. The experiment [23] evidences that phonon structure in superconducting state is preserved even if it is smeared out completely in the normal state spectra. Whether this is due to inelastic processes or strong-coupling virtual-phonon effects still remains to be clarified.

Strong nonlinearities of current-voltage characteristic of $N-c-S$ (c - constriction) at voltages $eV \leq \Delta$ are due to energy gap singularity in the electron density of state of superconductor. The Blonder-Tinkham-Klapwijk model [9] with Dynes extension $E \to E + i\Gamma$ [10] gives a good fit to the experimental data. Using this model one can show that the PC with nominally type-I superconductor (Zn) may acquire properties of the phase transition in magnetic field either of first or second order, depending on the contact preparation conditions [24].

We give an example of Andreev-reflection studies of energy gap in recently discovered magnetic superconductor $HoNi_2B_2C$ which shows complicated magnetic and superconducting phase diagrams. Two effects are clearly observed. First, when the sample possesses both spiral magnetic structure and superconducting order there is no clear cut gap. The gap appears at lower temperature when the phase transition to commensurate antiferromagnetic structure occurs [31]. Second, the Dynes parameter Γ shows strong energy dependence with a structure at $eV \simeq 4$ meV where the normal-state PC EPI spectrum shows a strong peak. We conclude that in the vicinity of Δ $\Gamma(eV)$ may give quite noticeable structure corresponding to low-energy boson excitations [33].

For many contacts with quite different superconducting material (normal metals, high-temperature superconductors, heavy-fermion compounds) one finds the BTK barrier strength parameter $Z \simeq 0.5$. We argue that quite probably all these contacts are in dirty limits which referring to clean BTK model gives the effective value of $Z = 0.55$. Thus, one usually applies the clean BTK model for fitting the dirty junctions which is questionable.

Finally, we discuss the van-Son-van-Kempen-Wyder experiment [36] which enables one to determine the spatial dependence of superconducting order parameter with the means of $N-c-S$ PC.

I. INTRODUCTION

We consider 3D constriction between two bulk metal electrodes. The characteristic dimension of a bridge is small compared with the inelastic mean free path (l_i) of charge carriers. These contacts (Fig.1) can be produced with two sharp edges of bulk electrodes (c) or by gently touching a sharpened needle to the flat surface (d) [1]. In a more controlled manner, a thin film point contacts (PC) are produced either by short-circuiting a thin oxide layer (a) [2], or by nanolithografical patterning (b) [3]. Another technique makes use of the so-called mechanically-controllable break junctions (e) [4].

As a model for these junctions a circular orifice with diameter d in impenetrable partition or a circular channel with a length L connecting two bulk electrodes are often used (Fig.2). The resistance in the ballistic limit ($l \to \infty$) is equal to (Fig.3):

$$R_N = R_q\left(\frac{16}{d^2k_F^2}\right);\ \text{where } R_q \simeq 12.9\ \text{k}\Omega$$

which serves for estimation of the contact size d. In the same figure the electron distribution function in momentum space is shown in the current state at the points

Adriatico Research Conference, 8-11 July '97, Miramare-Trieste, Italy.
"Superconductivity, Andreev Reflection, and Proximity Effects in Mesoscopic Structures"

inside the orifice [5]. In the quasi-ballistic regime (Fig.4) ($l > \max\{d, L\}$) the differential resistance $R = dV/dI$ at $T = 0$ in the normal state is equal to (Fig.6):

$$\frac{\Delta R(eV)}{R_0} = \frac{8}{6\pi}\frac{d}{l_i(eV)}$$

which for the second derivative of current-voltage characteristic (IVC) gives:

$$\frac{d\ln R(eV)}{d(eV)} = \frac{8}{3}\frac{ed}{\hbar v_F} g_{PC}(eV) \qquad (1)$$

where $g_{PC}(eV)$ is the electron-phonon interaction (EPI) function analogously to the Eliashberg EPI-function [6]. The EPI function can be expressed by $g(eV) = \alpha^2(eV)F(eV)$, where $\alpha^2(eV)$ is the averaged square of electron-phonon matrix element and $F(eV)$ is the phonon density of states.

In case of diffusive ($l_e \ll d$) but still spectroscopic ($d \ll \sqrt{l_i l_e}$) regime (Fig.5) the contact size d in (1) should be replaced by the elastic mean free path l_e [7]. Also the contact resistance is given by $R_M = \rho/d$ where ρ is the resistivity. For clean channel model ($d \ll L$) the diameter d in (1) should be replaced by $(3\pi/4)L$ (Fig.7). For the intermediate cases one can use the interpolation formulas. From the appearance and intensity of the EPI spectrum (1) one can judge about the chemical structure, average mean free path and the shape of the constriction. This is important since one often can't control the junction properly while producing.

If one of the electrodes become superconducting, then the quasiparticle incoming from the normal metal has a certain probability to find another electron to form a Cooper pair in the superconducting electrode. This process is called Andreev transformation [8] and leads to reflection in the normal metal the quasiparticle of opposite signs of charge and velocity but with the same excitation energy (Fig.8). The total current is the sum of normally and Andreev transmitted quasiparticles [9]:

$$I_{NS} = const \int_{-\infty}^{\infty} [f(E - eV) - f(E)] \times$$
$$\times [1 + A(E) - B(E)]\, dE$$

where $A(E)$, $B(E)$-probabilities of Andreev and ordinary reflections, respectively.

The experimental characteristic can be much better fit if one introduces the complex energy for quasiparticle excitation $E \rightarrow (E + i\Gamma)$ where Γ is the parameter smearing the stationary quasiparticle state [10]. The model introduces the arbitrary barrier strength at NS interface, Z, and since $A(E)$ depends on the superconducting energy gap Δ, the fit to the experiment gives three parameters as a result: Δ, Γ, Z. Similar phenomena occurs in $S-c-S$ junctions which can be considered as two $S-c-N$ junctions connected in series. This model was introduced by Blonder, Tinkham and Klapwijk (BTK-model) [9].

One of the distinguish feature of all models considering the conductivity of normal metal-constriction-superconductor ($N-c-S$) junctions is the appearance of the so-called excess current at $eV > \Delta$ [11,12] (Fig.9). The magnitude of excess current is very sensitive to the impurities or defects in a constriction distributed either homogeneously or as a barrier with a strength Z. On the other hand, BTK model with $Z = 0.55$ gives results very close to the dirty (diffusive) theory of Artemenko, Volkov and Zaitsev (AVZ) (Fig.10). We show below that the BTK model gives Z parameter very close to the "magic" value of about 0.5 for quite different superconductors and normal-metal counter electrodes. Probably this means that we often deal with the dirty superconductors nevertheless applying the ballistic BTK theory for fitting. Whether this fitting is correct remains to be answered, but it should be noted that BTK model gives quite good fit in any case.

II. EXCESS CURRENT

A. Dependence on purity

The parallel experimental study of EPI function in the normal state and the magnitude of the excess current in the superconducting state for $S-c-S$ junctions shows that the ratio of $l_e/d \simeq 0.5$ is enough to transform the clean $S-c-S$ junctions into the dirty one (see Figs.11,12).

In the upper panel of Fig.11 the solid line corresponds to the PC EPI spectrum for *normal* clean Sn-Sn junction which is directly recorded in the experiment [13]. The reconstructed EPI function from the *superconducting-tunneling* procedure of Rowell-McMillan is shown with a dot line [14]. The accordance between these two spectra are very good not only in the shape but also in the magnitude which proves that an idealized model of clean circular orifice describes the contact properties well. This was shown also for a number of other metals [1].

From the theory of PCS with elastic scattering in the contact region [15,7], one obtains the dependence of spectral intensity as a function of l_e/d for homogeneously distributed impurities (lower panel of Fig.11). For different Sn-Sn point contacts this enables us to estimated the ratio l_e/d . On the other hand, in the superconducting state for the same junctions we measure the magnitude of excess current, which according to the upper panel of Fig.12, remains constant up to V =4,5 mV. In Fig.12 we plot the deviations from Ohm's law of IVC in superconducting (curve 1) and normal (curve 2) states. The difference between them just corresponds the excess current. The dependence of the excess current on the maximum value of PC EPI function is shown in the lower panel of Fig.12. Here, by two dotted horizontal lines we show the limiting value for the excess current in the clean

and dirty state (see formulas in Fig.12). Since maximum value of $g_{PC}(eV)$ for Sn equals 0.406 [1], from to the graph $g_{PC}/g_{PC}^{\max}(l_e/d)$ in Fig.11 we find that $l_e/d \simeq 0.5$ is enough to transform the clean $S-c-S$ junctions into the dirty one. The PC spectroscopy enables us to conclude whether impurities are homogeneously distributed or they are located as a barrier at the interface, since the relative intensity of PC spectra does not saturate, when the concentration of homogeneously distributed impurities increases, unlike the excess current and Z-parameter.

B. Inelastic contribution to excess current

Let us consider the excess current at high voltages $eV \gg \Delta$ (Fig.13). Although it is often mentioned in the simplified theories that the excess current remains constant, in reality it quite noticeably depends on energy. According to the Refs. [16,17] one can write for the ICV in the superconducting state

$$I(V) = V/R - \delta I_{ph}^{N}(V) + I_{exc}(V) \qquad (2)$$

where

$$I_{exc}(V) = I_{exc}^{(0)} - \delta I_{ph}^{S},$$
$$\text{and } \delta I_{ph}^{S}(V) = \delta I_{el}^{S}(V) + \delta I_{in}^{S}(V).$$

Here $\delta I_{ph}^{N}(V) \sim I(V)\left(\frac{d}{l_i}\right)$ is the estimates of normal state nonlinearities considered above. There are two other components due to nonlinearities of excess current:

$$\delta I_{el}^{S}(V) \sim I_{exc}^{(0)}\left(\frac{\Delta(E)}{\hbar\omega_{ph}}\right),$$
$$\text{and } \delta I_{in}^{S}(V) \sim I_{exc}^{(0)}\left(\frac{d}{l_i}\right).$$

Let us focus on the second one. In $N-c-S$ junction at $T=0$ this term leads to the relation [18]:

$$\frac{1}{R}\frac{dR}{dV} = \frac{4ed}{3\pi}\sum_{\alpha=1,2}\frac{1}{v_F^{(\alpha)}}\int_0^{\infty}\frac{d\omega}{\Delta}S\left(\frac{\omega-eV}{\Delta}\right)g_{PC}^{(\alpha)}(\omega); \quad (3)$$

where α is the number of electrode constituting the contact,

$$S(x) = \theta(x-1)\frac{2(x-\sqrt{x^2-1})^2}{\sqrt{x^2-1}},$$

and $\theta(x)$ is the tetha-function.

For an infinitely narrow peak in the EPI function at energy $\hbar\omega_0$ the second derivative of IVC leads to the maximum with width of Δ shifted by Δ *to the lower energy*. This unexpectedly shift is due to relaxation of electron to hole appeared due to Andreev reflection. Inelastic processes with emission of real phonons occur when an electron quasiparticle with energy of the order of eV relaxes to the hole state appearing due to Andreev reflection of another electron with energy of the order of Δ (Fig.14).

On the other hand, if the phonon maximum in EPI function has a width $\delta\omega$ much greater than $\max(\Delta, T)$ then the S-function in formula (3) acts effectively as a δ-function, and the *differential conductance* of excess current is proportional to EPI spectral function $g_{PC}(eV)$:

$$\frac{1}{R(V)} - \left(\frac{1}{R(V)}\right)_{\Delta=0} = -\frac{8}{3R_0}\frac{d\Delta}{\hbar}\sum_{\alpha=1,2}\frac{1}{v_F^{(\alpha)}}g_{PC}^{(\alpha)}(eV),$$

$$\text{for } \delta\omega \gg \max(\Delta, T);$$

Let us consider the experiment aimed to observed above mentioned relations [19]. A pure enough Sn-Cu heterocontact is measured in normal and superconducting (Sn-)state. In normal state the PC EPI spectrum (solid curve 4) shows weighted by $\left[1/v_F^{(\alpha)}\right]$ contributions from Sn (curve 5) and Cu (curve 6) in Fig.15, corresponding to formula (3) in the limit $\Delta \to 0$ [20]. The original $d^2V/dI^2(V)$ is represented by curve 3 as recorded. When Sn becomes superconducting one sees a small shift of the main maximum *to the lower energy* by the magnitude of the order of Δ(Sn)=0.6 meV, followed by slight increase in the width and intensity of the spectrum. Note, that the excess current (curve 1) remains almost constant up to about 40 meV, where a transition to the nonequilibrium state with suppression of the superconducting order parameter occurs. Comparing the curves 2 and 3, we prove that in $S-c-N$ contact with the parameters: $d \ll \xi_0$; $d \ll l_i, l_e$; $\hbar\omega_{ph} \gg \Delta$ - the main contribution in formula (2) comes from the normal term $\delta I_{ph}^{N}(V)$ with slight modifications due to $\delta I_{in}^{S}(V)$ term.

C. Elastic contribution to excess current

Now consider the strong coupling superconductor Pb ($\hbar\omega_{ph} \geq \Delta$) in $S-c-N$ contacts with normal Ru and Os [21]. Both normal metals have very small phonon density of states in the low-energy range where the Pb-phonons have maxima. This enables us to neglect the contribution from the normal metal. The experimental curves are shown in Fig.16 (curves 2, 4) for two different contacts. The curve 2 corresponds to relatively clean contact for which the spectrum in the normal state is given by the dotted line (curve 3) *with the same ordinate scale*. One immediately sees that the phonon peaks are shifted to the *higher* energies roughly by Δ(Pb)$\sim$1.3 meV. Moreover, the intensity is higher than that in the normal state and it does not decrease much for noticeably dirtier contact (shown by curve 4). These properties contradict the inelastic contribution predictions.

Let us consider the elastic contribution for the excess current nonlinearities (term $\delta I_{el}^{S}(V)$ in formula (2)). For ballistic $S-c-N$ with the strong-coupling superconductor Omel'yanchuk *et al.* predict [17]:

$$\left\{\frac{dI}{dV}(eV)\right\}_{S-c-N} = \frac{1}{R_0}\left\{1+\left|\frac{\Delta(\varepsilon)}{\varepsilon+\left[\varepsilon^2-\Delta^2(\varepsilon)\right]^{1/2}}\right|^2\right\}_{\varepsilon=eV} \tag{4}$$

for the total differential conductance at $T=0$. The shape of this curve is schematically drawn in the right panel of Fig.16 for a Lorentzian phonon peak at $\hbar\omega_0$ in the EPI spectrum. The expression (4) is analogous to the Schrieffer [22] formula for tunneling junctions:

$$\left\{\frac{dI}{dV}(eV)\right\}_{S-I-N} = \frac{1}{R_0} Re\left\{\frac{\varepsilon}{\sqrt{\varepsilon^2-\Delta(\varepsilon)^2}}\right\}_{\varepsilon=eV},$$

which is used in the Rowell-McMillan-Dynes spectroscopy of EPI function in superconductors.

The order of magnitude of elastic nonlinear correction to the conductance is $[\Delta(\varepsilon)/\hbar\omega_{ph}]^2$ for $\Delta(\varepsilon) \ll \hbar\omega_{ph}$ just as in the tunneling spectroscopy. Since $I_{exc} \sim \Delta/R$ and the total current $I \sim \hbar\omega_{ph}/R$, the elastic correction to the contact current does not depend on the contact diameter d and has the order of $I_{exc}[\Delta(\varepsilon)/\hbar\omega_{ph}]$ which can be greater than the inelastic contribution $I_{exc}(d/l_i)$. One sees that in $N-c-S$ contacts with Pb the elastic term prevails (Fig.16) whereas in Sn-contacts the situation is opposite (Fig.15). In principle, the Eliashberg EPI-function can be extracted from point contact characteristic in the same way as in the tunneling spectroscopy [14], provided one should be sure that the inelastic term makes negligible contribution to the spectra.

D. Phonon spectra in dirty superconducting contacts

In dirty superconducting point contact the situation is vague. The experiment [23] evidences that phonon structure in superconducting state is preserved even if it is smeared out completely in the normal state. In the Fig.17 the IVC (curves S, N) of Nb-Nb junctions are shown in the superconducting and normal states, respectively. One sees that the excess current is almost constant for all energy range. Its magnitude approximately corresponds to the dirty $S-c-S$ junction [11]. The second derivatives of IVC (curves 1-4) have noticeable structure at the phonon energies $\hbar\omega_{TA}$ and $\hbar\omega_{LA}$ in the superconducting state which is completely smeared out in the normal state. The shape of the main peak corresponds to the maximum in differential resistance near $\hbar\omega_{TA}$. Whether this corresponds to the shifted to higher biases inelastic peak due to predictions of inelastic contribution (see formula (39) in [16]):

$$\left(\frac{dI_{exc}}{dV}\right)_{clean} = -\frac{1}{R_0}\frac{16}{3\pi}\left(\frac{d}{\xi_0}\right)\left[g^N(eV)+g^S(eV)\right],$$

$$\text{for } (\delta\omega \gg \Delta);$$

where $g^N(eV)$ is the PC EPI function for the normal state and $g^S(eV)$ differs from that only in different $K-$factor [16], or we observe an elastic contribution due to suppression of inelastic component with a factor (l_e/d), remains unclear. Still, the fact that we could observe quite noticeable phonon structure in the dirty superconducting contact is encouraged.

III. ANDREEV-REFLECTION SPECTRA OF SUPERCONDUCTING ENERGY GAP

A. Change of the order of phase transition

The strong nonlinearities of IVC of $N-c-S$ contacts at voltages $eV \le \Delta$ are due to the singularity in the electron density of state near the superconducting gap-edge. The BTK-model [9] with Dynes extension [10] (BTKD) gives a good fit to the experimental data. Using this model one can analyze some of the unexpected properties of the superconducting contacts.

In Fig.18 the Andreev-reflection spectra ($dV/dI(V)$-dependences) in the range $|eV| \le \Delta$ are shown for the $N-c-S$ contacts Ag-Zn [24]. Zn is a type-I superconductor, and its behavior in the upper two panels of Fig.18 corresponds to the first-order phase transition in magnetic fields between 4.06 and 4.15 mT. On the other hand, the contact which characteristics are shown in the lower two panels of Fig.18, reveals gradual decrease of the superconducting energy-gap structure up to field of several times greater than $B_{c,bulk}$. The BTKD-fits for these two contacts give the energy-gap Δ- and Γ-parameters shown in Fig.19. One should notice the almost constant Γ- and Δ-parameters in the first case, whereas the greatly increased Γ and smoothed Δ-decrease is observed in the second case. The latter could be expected if the vortex structure exists near the contact, and $\Delta(H)$-dependence is compared roughly with that for thin film $\Delta \propto \left[1-(B/B_c)^2\right]^{1/2}$ [25] (solid line) and bulk type-II superconductor $\Delta \propto [1-(B/B_c)]^{1/2}$ [26] (dash-dotted line) . Naturally, one expects the increase of $\Gamma(H)$ in the mixed state. Assuming in the latter case we obtain a dirty region near the contact, one can obtain the elastic mean free path, coherence length, penetration depth from enhancement of B_{c2} through the formulas [27]:

$$l_e \sim \Phi_0/2\pi\xi_0 B_{c2};$$

$$\xi \sim (\xi_0 l_e)^{1/2};\ \lambda \sim \lambda_L (\xi_0/l_e)^{1/2};$$

and shows that for the second-order phase transition there is always $\xi < \sqrt{2}\lambda$..

It is worth to note that the temperature dependences of Δ correspond in both cases to BCS curve with little deviations, although $\Gamma(B = 0)$-parameter can differ several times. The uncorrelated behavior of Γ and Δ shows that there is no depairing in the bulk. This point of view is supported by the dependence of Γ on contact resistance (i.e., on contact size) (see Fig.19, lower graph). An increase of resistance is followed by an increase of Γ pointing to the interface origin of this parameter. Interestingly, that in the normal UPt_3 the increase of Γ is much larger than for Ag as a counter electrode with superconducting Zn which probably is connected with antiferromagnetic order in UPt_3. Probably, at the interface of magnetic heavy-fermion compounds the strong uncompensated magnetic field causes the pair breaking [24]. In spite of this, a successful study of anisotropy of the superconducting energy gap in UPt_3 was carried out [28].

B. Energy dependence of depairing parameter $\Gamma(eV)$

Another case with large magnetic depairing shows the $HoNi_2B_2C$ superconductor. This recently discovered material has a layered tetragonal structure similar to the high-T_c superconductors, although being electronically three-dimensional. The conducting (and superconducting) layers of Ni_2B_2 are intercalated with the magnetic HoC layer where at the lower temperatures the Ho-magnetic moments are ordered ferromagnetically. Along the c-axis, below about 8 K, the spiral magnetic order exists which changes to the commensurate antiferromagnetic below $\sim$ 5 K (Fig.20) [29]. The superconductivity starts at about the same temperature (8 K) as the magnetic order. The competition between superconducting and spiral magnetic order leads to pronounced minimum on the $B_{c2} - T$ superconductor-normal-metal phase diagram [30]. When studied by Andreev-reflection spectroscopy, the dV/dI-characteristics show absence of pronounced energy gap in the temperature interval where the spiral magnetic order coexists with superconductivity, albeit the clear appearance of the gap in the temperature interval where the superconductivity coexists with the commensurate antiferromagnetism (Fig.21) [31]. Interestingly, the excess current, which is proportional to the area between $dV/dI(V)$-curves in normal and superconducting states, has not strong minimum near T_c^* where the gapped superconductivity appears, unlike the zero-voltage resistance which reflects the density of electron states at the Fermi level (Fig.22). In the gapless region excess current comes to T_c linearly: $I_{exc} \propto (1 - T/T_c)$ instead of having square-root singularity for the gapped superconductor: $I_{exc} \propto \Delta(T) \propto (1 - T/T_{c0})^{1/2}$ [32]. Still, even at low temperature the Γ-parameter is high enough, probably, due to uncompensated local internal magnetic field causing depairing effect (Fig.23) [33].

At bias $|eV| \approx 4$ meV there is a kink in a $dV/dI(V)$-characteristic which also present in other superconducting compounds of the same homological row: $ErNi_2B_2C$ and YNi_2B_2C (Fig.24) [33]. This sudden increase of the width of Andreev-reflected structure points to the increase of Γ-parameter at this energy. This increase should correspond to the strong peak in EPI spectral function. Indeed, the normal-state investigation of $HoNi_2B_2C$ and YNi_2B_2C by means of inelastic PC spectroscopy reveals strong phonon peaks at this energy (Fig.25) [33] which corresponds well the neutron data showing the softening of phonon modes with maximum in density of states at $eV \simeq 4$ meV [34,35]. Other peaks in the PC spectra also correspond well to the neutron data (Fig.26).

C. Spatial dependence of the superconducting order parameter

In Ref. [36] van Son, van Kempen and Wyder develop a new method to study the proximity effect at the normal-metal-superconductor interface. This method uses Andreev reflections from the remote $N - S$ interface which contribute to the excess current in the $N - c - N$ contact (Fig.27). Since electron mean free path is comparable to the N-film, the ballistically propagated electron quasiparticles are reflected as a hole from the $N - S$ interface and contribute to the excess current whatever the propagation direction is. A schematic diagram for coordinate dependence of Δ is shown in Fig.27 . The superconducting order parameter (Δ in the bulk) experiences the jump at the $N - S$ interface and then decreases to zero at a distance ξ_N into the normal metal. We may roughly distinguish two cases. First, when the thickness of the normal layer $d \ll \xi_N$, we have $N - c - S'$ contact with slightly depressed energy gap at the contact interface. This corresponds to the left panel of graphs shown in Fig.27, with a double minimum structure of $dV/dI(V)$ which is a hallmark of AR at the $N - S$ interface of a metallic PC with a small barrier [9]. Another case corresponds to $d \gg \xi_N$ and is shown in the right panel of Fig.27. There one can distinguish two features: 1) a zero-bias minimum which comes from the tail of order parameter in the normal metal, and 2) - a smaller minima originating from the gap in the bulk superconductor S ($eV \approx \pm 1.3$ meV in Pb). The intensities of dV/dI-structures are greatly reduced due to the scattering of Andreev-reflected quasiparticles by static defects. If one assumes the probability of the ballistic propagation equals to:

$$\Lambda(eV) = \frac{1}{\pi}\int_0^{2\pi} d\phi \int_0^{\pi/2} d\theta \sin\theta\cos\theta \exp\left[\frac{-2d'(eV)}{l\cos\theta}\right],$$

then the shape of $R(V) = dV/dI(V)$ curve (at $T = 0$) takes the form:

$$\frac{R(V)}{R_N} = [1 + A(eV)\Lambda(eV)]^{-1};$$

where $A(eV)$ is the AR probability and R_N is the normal-state contact resistance.

From the intensities of zero-bias and bulk energy-gap structure one estimates two parameters l and d' (see Table in Fig.27) and obtains self-consistently that $(d-d'(0))$ is approximately constant and corresponds in order of magnitude to the $\xi_N = \left(\frac{\hbar v_F l}{6\pi k_B T}\right)^{1/2} \approx 0.4$ μm. In principle, this experiment can be used to reconstruct the position dependence of the pair potential near the $N-S$ interface.

IV. CONCLUSIONS

Since the properties of the 3D metal in point contacts can differ quite noticeably from the bulk , we conclude that in order to characterize them, the Andreev reflection study in the superconducting state should be carried in parallel with the normal-state point-contact spectroscopy. In particular, many contact for which one applies the BTKD model are in the dirty state and it is not easy to determine whether they have uniform distribution of impurities or those are concentrated at the interface as a barrier.

The energy gap and superconducting order parameter can be studied as a function of temperature and magnetic field, using the BTKD model. One should not be surprise if the properties of superconductors under the contact differ from that in the bulk. Only the properly prepared contacts with well characterized properties have reproducible characteristic and can be reliably investigated as represented the bulk material.

The energy dependence of excess current in superconducting state provides a tool to study excitations by which Cooper pairs are bounded. This properties are inexpensively when there is no possibility to study point contact spectra in the normal state, or in dirty metals when the PC spectra are very weak and smeared.

This work is supported by European Community grant INTAS-94-3562. The author is grateful to Physikalisches Institut of Karlsruhe University for hospitality in the frame of Humboldt-Forschungspreisträger Program.

[1] I.K. Yanson, A.V. Khotkevich, *Atlas of Point-Contact Spectra of Electron-Phonon Interaction in Metals* (in Russian), Naukova Dumka, Kiev, 1986, 144 pages; [Engl. transl: A.V. Khotkevich, I.K.Yanson, *Atlas of Point-Contact Spectra of Electron-Phonon Interaction in Metals*, Kluwer Academic Publishers, (1995), 151 pages]

[2] I.K. Yanson, Yu.N. Shalov, Electron-phonon interaction spectrum in copper, Sov. Phys. JETP, **44**, 2148 (1976).

[3] K.S. Ralls, R.A. Buhrman, and R.C. Tiberio, Appl. Phys. Lett. **55**, 2459 (1989).

[4] C.J. Muller, J.M. van Ruitenbeek, and L.J. de Jongh, Physica C **191**, 485 (1992); Phys. Rev. Lett. **69**, 140 (1992).

[5] I.K. Yanson, Physica Scripta, **T23**, 88 (1988).

[6] I.O. Kulik, A.N. Omel'yanchuk, and R.I. Shekhter, Fiz. Nizk. Temp. **3**, 1543 (1977) [Sov. J. Low Temp. Phys. **3**, 740 (1977)].

[7] I.O. Kulik, R.I. Shekhter, and A.G. Shkorbatov, Zh. Eksp. Teor. Fiz. **81**, 2126 (1981) [Sov. Phys. JETP **54**, 1130 (1981)].

[8] A.F. Andreev, Zh. Eksp. Teor. Fiz. **46**, 1823 (1964) [Sov. Phys. JETP **19**, 1228 (1964)]

[9] G.E. Blonder, M. Tinkham, and T.M. Klapwijk, Phys. Rev. B **25**, 4515 (1982).

[10] R.C. Dynes *et al.*, Phys, Rev. Lett. **41**, 1509 (1978).

[11] S.N. Artemenko *et al.*, Solid State Communs. **30**, 771 (1979).

[12] A.V. Zaitsev, Zh. Eksp. Teor. Fiz. **78**, 221 (1980); **79**, 2015 (1980); **86**, 1742 (1984) [Sov. Phys. JETP **51**, 111 (1980); **52**, 1018 (1980); **59**, 1015 (1984)]

[13] A.V. Khotkevich, I.K. Yanson, Fiz. Nizk. Temp. **7**, 727 (1981) [Sov. J. Low Temp. Phys. **7**, 354 (1981)].

[14] W.L. McMillan and J.M. Rowell, in: *Superconductivity* (ed. by R.D. Parks), Vol.1, Marcel Dekker, New York (1969), p.561.

[15] I.O. Kulik, I.K. Yanson, Fiz. Nizk. Temp. **4**, 1267 (1978) [Sov. J. Low Temp. Phys. **4**, 596 (1978)].

[16] V.A. Khlus, A.N. Omel'yanchuk, Fiz. Nizk. Temp. **9**, 373 (1983) [Sov. J. Low Temp. Phys. **9**, 189 (1983)].

[17] A.N. Omel'yanchuk *et al.*, Fiz. Nizk. Temp. **14**, 1142 (1988) [Sov. J. Low Temp. Phys. **14**, 630 (1988)].

[18] V.A. Khlus, Fiz. Nizk. Temp. **9**, 985 (1983) [Sov. J. Low Temp. Phys. **9**, 510 (1983)].

[19] I.K. Yanson *et al.*, Fiz. Nizk. Temp. **10**, 423 (1984) [Sov. J. Low Temp. Phys. **10**, 220 (1984)].

[20] R.I. Shekhter and I.O. Kulik, Fiz. Nizk. Temp. **9**, 46 (1983) [Sov. J. Low Temp. Phys. **9**, 22 (1983)].

[21] A.V. Khotkevich *et al.*, Fiz. Nizk. Temp. **16**, 1199 (1990) [Sov. J. Low Temp. Phys. **16**, 693 (1990)].

[22] J.R. Schrieffer, *Theory of Superconductivity*, Benjamin, New York (1964).

[23] I.K. Yanson *et al.*, Solid State Communs **50**, 515 (1984).

[24] Yu.G. Naidyuk *et al.*, Phys. Rev. B **54**, 16077 (1996).

[25] M. Tinkham, *Introduction to Superconductivity* (McGraw-Hill, New York, 1980), p.125.

[26] K. Maki, in *Superconductivity*, edited by R.D. Parks (Marcel Dekker, New York, 1969), Vol.2, p.1035.

[27] P.-G. de Gennes, *Superconductivity of Metals and Alloys*, W.A. Benjamin, Inc. New York 1966.

[28] G. Goll *et al.*, Phys. Rev. Lett. **70**, 2008 (1993); Phys.

Rev. B **52**, 6801 (1995).
[29] T.E. Grigereit *et al.*, Phys. Rev. Lett. **73**, 2756 (1994).
[30] P.C. Canfield *et al.*, Physica c **230**, 397 (1994).
[31] L.F. Rybaltchenko *et al.*, Europhys. Lett. **33**, 483 (1996).
[32] S.I. Beloborod'ko, A.N. Omel'yanchuk, Fiz. Nizk. Temp. **17**, 994 (1991) [Sov. J. Low Temp. Phys. **17**, 518 (1991).
[33] I.K. Yanson *et al.*, Phys. Rev. Lett. **78**, 935 (1997); Fiz. Nizk. Temp. **27**, No.9 (1997) [Low Temp. Phys. **27**, No.9 (1997)].
[34] P. Dervenagas *et al.*, Phys. Rev. B **52**, R9839 (1995).
[35] H. Kawano *et al.*, Phys. Rev. Lett. **77**, 4628 (1996).
[36] P.C. van Son *et al.*, Phys. Rev. Lett. **59**, 2226 (1987).

FIG. 1. 3D point contacts. (a) Thin film tunnel structure with short through the oxide; (b) litographically made thin film structure; the contact size is made in a controlled manner; (c) , (d) pressure-type bulk point contacts in the "edge-edge" and "needle-anvil" geometry, the electrodes can be single crystals with known orientation; (e) mechanically-controllable break junction: 1 - a bar of a sample with a notch (2) in the middle, (3) Staycast with which the sample is glued to the bending beam (substrate) (4), vertical movement of the rod (5) break and re-establish the contact.

FIG. 2. Idealized models of 3D point contact. Most of formulas in the text are given for the orifice model.

FIG. 3. Schematic of electron flow through the orifice with diameter d in the ballistic regime. Below, the electron distribution function in momentum space is shown at the points inside the orifice in current carrying state. The bias eV is applied between electrodes.

FIG. 4. The schematic diagram illustrating the quasi-ballistic regime of current flow. The electrons passing through the orifice experience rare scattering by static imperfections (mean free path l does not depend on energy), dynamic quasiparticles with $l = l(eV)$ (e.g. phonons), and other energy-dependent scatterers (like Kondo-paramagnetic centers, which cross-section depends on the distribution function $f(\varepsilon, eV)$). The backscattering due to emission of quasiparticle with momentum q and energy $\hbar\omega \leq eV$ is shown which contributes to the nonlinearities of current-voltage characteristics.

FIG. 5. Diffusive regime of current flow. Point-contact spectroscopy is still possible provided the inequality written above holds. The nonequilibrium distribution function for electrons is shown below. The states below $\varepsilon_F - \frac{eV}{2}$ are occupied while those above $\varepsilon_F + \frac{eV}{2}$ are empty. The states inside the layer of eV are partially occupied with some asymmetry in the direction of current flow. R_M is the resistance of circular orifice in the diffusive regime, ρ is the resistivity.

FIG. 6. Some formulas for the quasi-ballistic and diffusive spectroscopic regimes of current flow. l is electron mean free path, l_e is the elastic mean free path, d, L are the diameter and length of a constriction (see Fig.2), ρ is resistivity. τ_{PC} and l_{PC} are mean free time and path taking into account the kinematic restriction imposed by contact geometry. v_F is Fermi velocity. Point-contact electron-phonon interaction (EPI) function $g_{PC}(\omega)$ is the product of averaged square EPI matrix element $\alpha^2(\omega)$ and phonon density of states $F(\omega)$. Λ_{in} is electron energy relaxation length, $\Delta R(eV)$ is the increase of energy-dependent differential resistance, and R_0 is the zero-bias resistance. In the diffusive regime the contact diameter should be replaced by elastic mean free path.

FIG. 7. Spectral intensities for idealized contact models. $\langle K \rangle$ is the form-factor for different models. $R = dV/dI(V)$. The models assume circular cross section.

FIG. 8. Andreev reflection at the interface of normal-metal-constriction-superconductor ($N - c - S$) contact. $f(E)$ is Fermi function, C is constant.

FIG. 9. Some examples of clean (with a barrier of strength Z) and dirty $N - c - S$ contacts. ξ_0 is the coherence length in clean superconductor.

FIG. 10. $dI/dV(\epsilon = eV)$-characteristics for clean ($Z = 0$, solid line) and dirty (dashed line) $N - c - S$ contacts. BTK-model with $Z = 0.55$ (thin solid line) and tunneling junction ($Z = \infty$, $S - I - N$ contact, dotted line) are shown for comparison.

FIG. 11. Upper panel: solid line - point-contact spectrum of electron-phonon interaction in Sn. The dots show the EPI spectral function reconstructed from superconducting tunneling [14]. Horizontal bar show energy resolution determined by the temperature. Lower panel: the decrease of the intensity of EPI spectrum lines as a function of the ratio of elastic electron mean free path to contact diameter [7].

FIG. 12. Upper panel: Current-voltage characteristics in superconducting 1 and normal 2 states. The zero-bias resistance R_0 is compensated by the bridge method. The difference between two curve gives the excess current $I_{exc}(eV)$. The theoretical formulas for the excess current in $S - c - S$ dirty and clean contacts [11,12]. Lower panel: The dependence of excess current on the maximum intensity in the PC EPI spectra of Sn.

FIG. 13. The energy dependence of excess current at high (compared to Δ) biases. R is normal-state resistance, $\delta I^N_{ph}(V)$ is the normal-state nonlinearities of IVC , while $\delta I^S_{ph}(V)$ corresponds to nonlinearities of the excess current. In the lower part, left panel, the $-d^2I/dV^2(V)$ of the inelastic $\delta I^S_{in}(V)$ component of $\delta I^S_{ph}(V)$ is shown for the infinitely narrow ($\delta\omega \ll \Delta$) phonon peak (shown as a thick vertical line) at $\hbar\omega_0 = 10\Delta$ (Δ is the energy gap). The same characteristic is shown for wide phonon peak ($\delta\omega \gg \Delta$) in the right panel. Theoretical formulas and the figures concern $N-c-S$ contact.

FIG. 14. The diagram showing the inelastic electron relaxation emitting phonons with the energy greater than eV. The second derivative of $N-c-S$ IVC differs from zero for biases smaller than $(\hbar\omega_0 - \Delta)$ (see Fig.13).

FIG. 15. Inelastic scattering via Andreev reflection. Experimental dependences for Sn-Cu heterocontact with $R_0 = 8.8\ \Omega$: 1) dependence $I_{exc}(V)eR_0/\Delta$; 2) and 3) - point-contact spectra in superconducting and normal states of the tin electrode, respectively; the scales for both curves are the same. 4) (solid curve) The point-contact EPI function obtained by subtraction of background from the curve 3). The dotted line show the theoretically expected PC EPI function obtained by adding PC EPI functions for tin (curve 5) and copper (curve6). $T = 1.5$ K. In normal state the superconductivity of tin is destroyed by magnetic field.

FIG. 16. The elastic contribution to nonlinearities of $N-c-S$ contact. The formulas are from Ref. [17] The right panel shows schematically the theoretical dependence of normalized differential conductivity (solid line in graph (b)) for the energy dependences of real (solid line) and imaginary (dashed line) part of superconducting order parameter simulating by Lorentzian phonon peak at $\epsilon = \hbar\omega_0$ [17]. Δ_0 is the energy gap. The left panel shows the comparison of calculated (curve 1) and experimental (3,5) PC spectra for $N-c-S$ contacts. The calculated curve uses $\Delta(\epsilon)$-function for strong-coupling superconductor Pb [14], while the dash-dotted curve shows the BCS $\Delta(\epsilon) = \Delta_0$ dependence. Curves 2 and 4 present the $d^2V/dI^2(V)$ for Pb contacts with single crystalline Ru and Os, and correspond to the clean and dirty junctions, respectively. Curve 3 shows the PC EPI spectrum of contact 2 in the normal state. The scale on Y-axis for curves 2 and 3 is the same. $T = 1.7$ K, superconductivity of Pb in curve 3 is destroyed by magnetic field.

FIG. 17. Point-contact spectra (d^2V/dI^2-dependences 1-4) of niobium junction with $R_0 = 30\ \Omega$. Curves 1,2,3, and 4 correspond to temperatures 4.4, 6.5, 8.65, and 10.6 K, the latter is above T_c. $I-V$ curves in superconducting (S) and normal (N) states are taken at 7.8 and 11.2 K, respectively. Niobium electrodes are covered by aluminium oxide [23]. The diagram shows that chemical potentials of Cooper pairs $\mu_{L,R}$ (shifted by eV) are different from chemical potential of quasiparticles μ_Q due to longitudinal penetration of electric field in superconducting electrodes. In the centre of the contact the phase-slip center (PSC) forms. Below presented formulas for clean $S-c-S$ contact [16], and decreased by $\frac{l_a}{d}$ times intensity of normal-state PC spectrum for dirty contacts compared to the clean one.

FIG. 18. Change of the order of phase transition in superconductor under the contact [24]. Upper panel: dV/dI curves vs V (dots) for Ag-Zn contact with $R_0 = 0.5\ \Omega$ and $T_c = 0.82$ K (a) for different temperatures T and (b) in different magnetic field B. Fit parameters for the theoretical curve [9] (dashed line) at $T = 0.06$ K are $\Delta = 110\ \mu$eV, $\Gamma = 6\ \mu$eV, and $Z = 0.5$. The fit curves are almost indistinguishable from the data also for higher temperatures and are therefore not shown. Lower panel: dV/dI curves vs V (dots) for Ag-Zn contact with $R_0 = 0.47\ \Omega$ and $T_c = 0.83$ K (a) for different temperatures T and (b) in different magnetic field B. Fit parameters for the theoretical curve [9] (dashed line) at $T = 0.06$ K are $\Delta = 124\ \mu$eV, $\Gamma = 6.5\ \mu$eV, and $Z = 0.51$.

FIG. 19. Upper panel: $\Delta(B)$ (triangles) and $\Gamma(B)$ (rectangles) at $T = 0.06$ K for contact shown in upper (a) and lower (b) panels of Fig.18. Solid and dash-dotted lines in (b) are $\Delta \propto \left[1-(B/B_c)^2\right]^{1/2}$ [as for thin films (Ref. [25])] and $\Delta \propto 1-(B/B_c)^{1/2}$ [as for type-II superconductor (Ref. [26])]. Dashed lines are guides to the eye. Lower panel: Dependence of the parameter Γ on the contact resistance $R_N = R_0$ for Zn-Ag and Zn-UPt_3 $S-c-N$ contacts. Solid lines are guides to the eye.

FIG. 20. $HoNi_2B_2C$ (a) crystal structure; (b) commensurate antiferromagnetic structure; (c) spiral magnetic structure [29].

FIG. 21. Temperature dependences of Andreev reflection spectra of $HoNi_2B_2C$-Ag $S-c-N$ contact. Dashed and dotted lines are guides to the eye. In the temperature range 8.6 - 5.5 K the gapless superconductivity is seen.

FIG. 22. Upper panel: dV/dI characteristics for a $HoNi_2B_2C$-Ag PC with $R_0 = 0.87\ \Omega$. Temperatures from bottom to top are 5.0, 6.0, 6.2, 6.4, 6.8, 7.2, 8.0, 8.4, 8.8, 9.0 K. The inset shows the excess current which is proportional the area between the normal and superconducting spectra, and decrease of zero-bias resistance in superconducting state. Lower panel: Temperature dependences of excess current (squares) and zero-bias resistance difference (circles) for PC whose characteristics are shown above. The lines are a guide to the eye.

FIG. 23. The fits with BTKD-model [9,10] for YNi_2B_2C-Cu and $HoNi_2B_2C$-Ag contacts at low temperatures. SF is an additional parameter which scales Y-axis to the experiment.

FIG. 24. dV/dI-curves for superconducting $HoNi_2B_2C$, $ErNi_2B_2C$ and YNi_2B_2C in contact with the normal metal showing the kinks at about $eV \approx \pm 4$ meV, which correspond to the peak in the EPI function [33].

FIG. 25. Low-energy phonon part of PC EPI spectra in the normal state for YNi_2B_2C and $HoNi_2B_2C$. The V_{2F} is proportional to second derivative of $I - V$ characteristic [33].

FIG. 26. The Δ_4 [ξ00] branches of phonon dispersion curves for $LuNi_2B_2C$ at 295 and 10 K [34]. The lines through the 10 K points are intended as guides to the eye. The arrows point to phonon peaks found from the PC spectra.

FIG. 27. Van-Son-van-Kempen-Wyder method to study the proximity effect at the normal-metal-superconductor interface. Schematic experimental setup. At any direction emitted quasiparticles from the point contact are backscattering via the Andreev reflection. Position dependence of Δ near an $N - S$ interface. The thickness of the N layer is d, while d' is an effective thickness of the nonsuperconducting layer. Left panel: Measured differential resistance vs voltage of a point contact on a Ag-Pb bilayer for two samples with different Ag-film thicknesses. The PC resistances are $R_S = 46\ \Omega$ ($d = 0.02\ \mu$m) and $R_S = 17\ \Omega$ ($d = 0.2\ \mu$m). The curve with $d = 0.2\ \mu$m has been shifted upward for clarity. The dashed line is a theoretical [9] curve. Right panel: Measured differential resistance vs voltage of a point contact on a Ag-Pb bilayer for three samples with different Ag-film thicknesses. The PC resistances are $R_S = 1.6\ \Omega$ ($d = 0.4\ \mu$m), $R_S = 1.2\ \Omega$ ($d = 0.7\ \mu$m), and $R_S = 4.3\ \Omega$ ($d = 0.9\ \mu$m). Note the different vertical scales. Table I. Mean free path l and effective thickness $d - d'(0)$ of the superconducting layer in N that are deduced from the measurements shown in the above figures.

Fig.1

3D constrictions

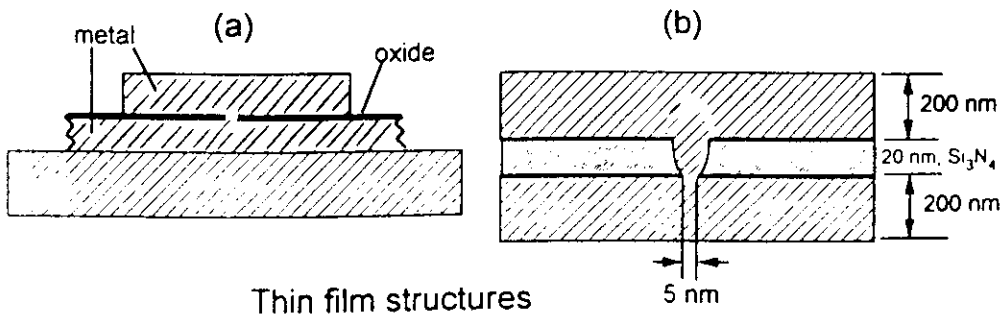

Thin film structures

Bulk electrode junctions:

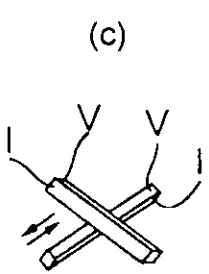

"edge-edge"

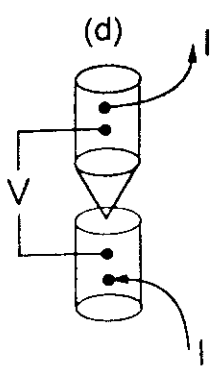

"needle-anvil"

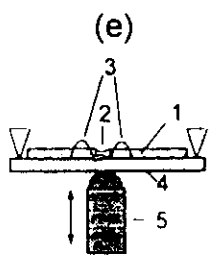

MCB

Models

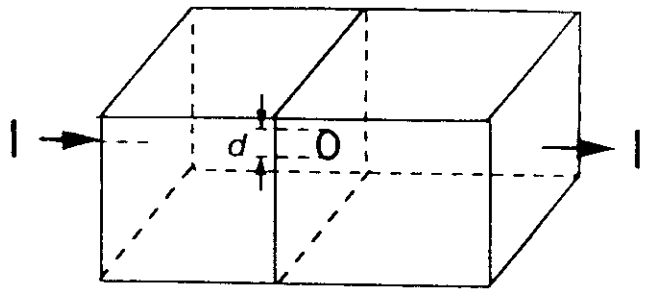

Orifice

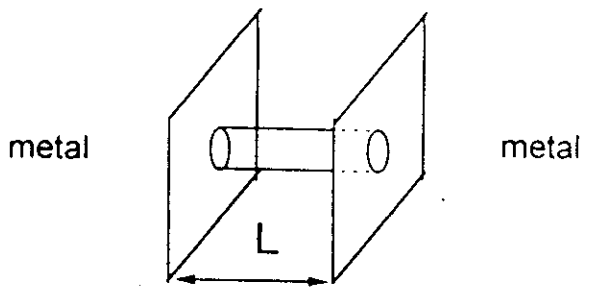

Channel (tube)

Fig.2

Ballistic regime

$l >> \max\{d, L\}$

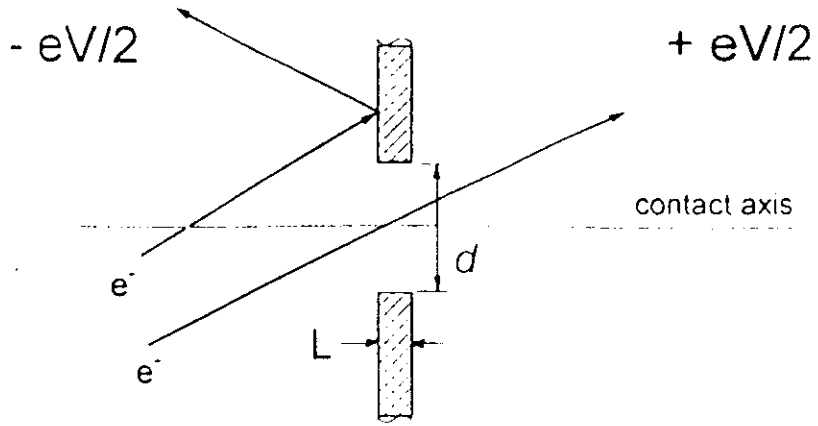

$G = G_q [S/(4\pi / k_f^2)]$; $G_q = 2e^2/h$

$R_{Sh} = R_q [16/(d^2 k_f^2)]$; $R_q = 12.9\ k\Omega$

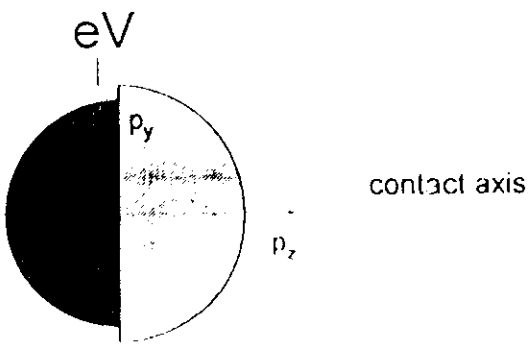

nonequilibrium electron distrubution function

$k_B T << eV << \varepsilon_F$

Fig.3

Quasi-ballistic regime

$l > \max\{d, L\}$

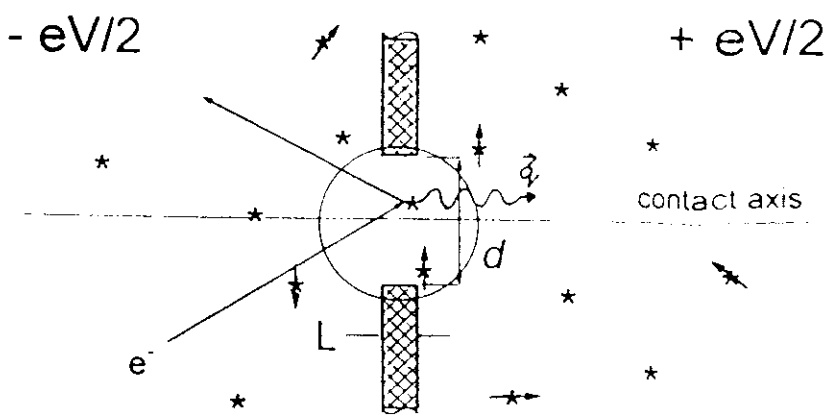

$\hbar\omega \leq eV$

Scatterers:

static - $l(eV) = \text{const}$

dynamic - $l(eV) = \Phi(eV)$

Kondo: - $l(eV) = \Psi[f(\varepsilon, eV)]$

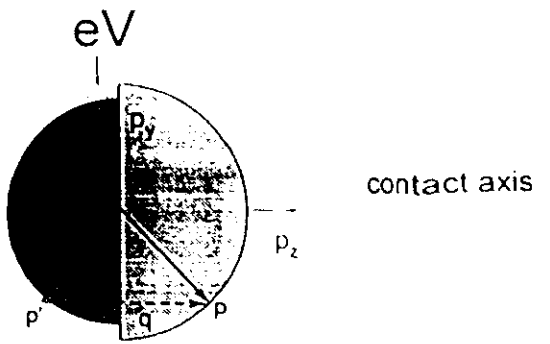

nonequilibrium electron distrubution function

$k_B T << eV << \varepsilon_F$

Fig.4

Diffusive regime

$l_e << \max\{d,L\} << \Lambda_{in}=(l_e l_{in})^{1/2}$

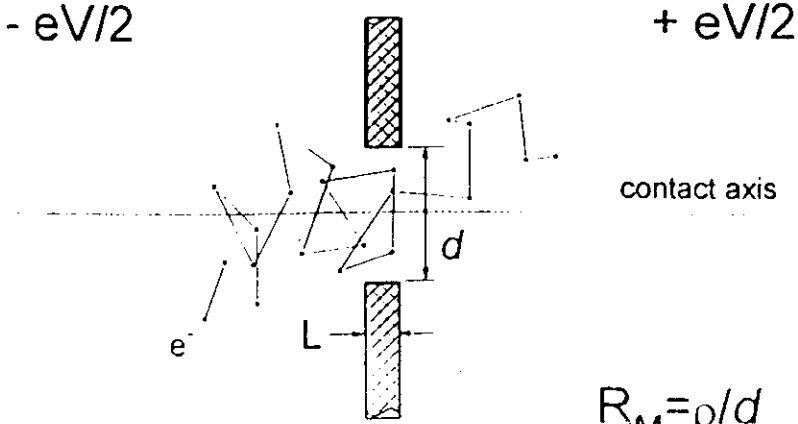

$R_M=\rho l/d$

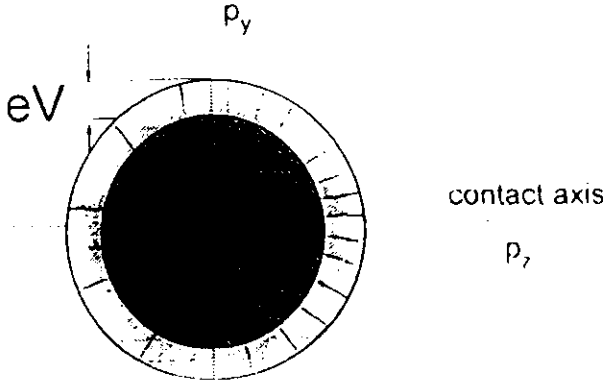

nonequilibrium electron distribution function

$k_B T << eV << \varepsilon_F$

Fig.5

Phonon scattering

Quasi-ballistic regime (T=0)

$l > \max\{d,L\}$

$R = (\rho l / d^2)\,(1 + d/l)$; $\quad l^{-1} = l_e^{-1} + l(eV)^{-1}$

$$\Delta R(eV) / R_0 = (8/6\pi)\, d / l_{PC}(eV)$$

$$l_{PC}(eV)^{-1} = 1/(v_F \tau_{PC}(eV)) = (2\pi/\hbar v_F)\int_0^{eV} g_{PC}(\hbar\omega)\, d(\hbar\omega)$$

$g_{PC}(\omega) = \alpha^2_{PC}(\omega) F(\omega)$; $\quad F(\omega)$ - density of phonon states

$$d\, lnR(eV)/d(eV) = (8ed/3\hbar v_F)\, g_{PC}(\hbar\omega); \quad (\hbar\omega = eV)$$

Diffusive regime $(l_e << d << \Lambda_{in})$

$$\Delta R(eV) / R_0 = (8/6\pi)\, l_e / l_{PC}(eV)$$

$$d\, lnR(eV)/d(eV) = (8el_e/3\hbar v_F)\, g_{PC}(\hbar\omega); \quad (\hbar\omega = e$$

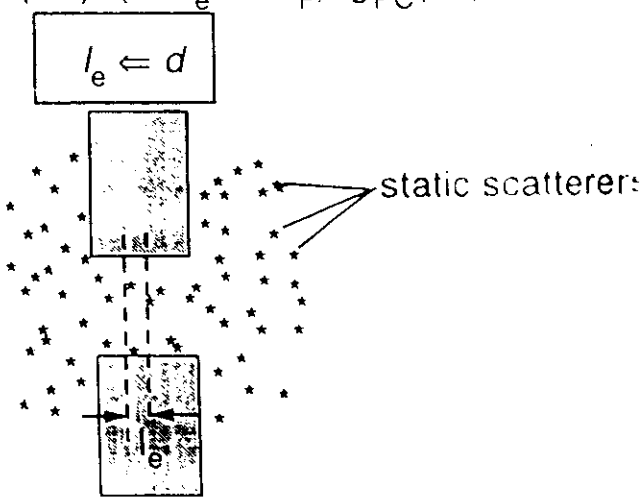

Fig.6

EPI spectral intensities

$$d\,(\ln R)\,/\,dV = (32/3)\,\{e[d\langle K\rangle]\,/\,\hbar v_F\}\,g_{PC}(eV)$$

Model	$[d\langle K\rangle]$	
clean orifice	$(1/4)\,d$	$(l \gg d \gg L)$
clean channel	$(3\pi/16)\,L$	$(l \gg L \gg d)$
dirty orifice	$(3\pi/16)\,l_e$	$(l_e \ll d)$
dirty channel	$(3\pi/16)\,l_e$	$(l_e \ll L)$

Linear interpolation for clean contact:

$$d\,(\ln R)\,/\,dV = -\,(8/3)\,[e g_{PC}(eV)/\,\hbar v_F]\,[d+(3\pi/4)L]$$

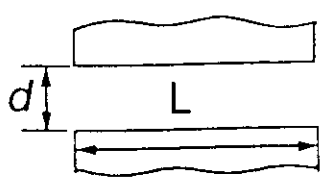

intens-1.org

Fig.7

Point-contact spectroscopy in the superconducting state

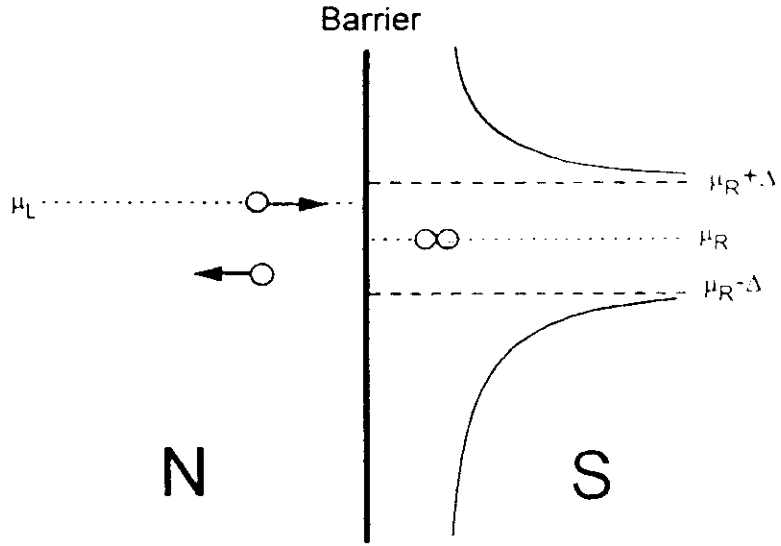

Andreev reflection between a normal metal and a superconductor. The upper quasiparticle incoming from the left faces the gap, and depending on the transparency there is a certain probability that it finds an electron to form a Cooper pair in the right electrode

$$I_{NS} = C\int_{-\infty}^{\infty}[f(E-eV) - f(E)][1 + A(E) - B(E)]\,dE$$

A(E) , B(E) - probabilities of Andreev and ordinary reflections, respectively.

$$E \rightarrow (E + i\Gamma)$$ Dynes *et al.*, Phys. Rev. Lett. 53, 2437 (1984)

Z : barrier strength,
$\Gamma(eV)$ = const: smearing parameter,
Δ: energy gap.

Artemenko, Volkov, Zaitsev [SSC 30, 771 (1979)]; Zaitsev [Sov. Phys. JETP 51, 111 (1980)]
Blonder, Tinkham, Klapwijk (Phys. Rev. 25, 4515 (1982))

andreev1.org

Fig.8

Current-voltage characteristics of S - c - N junction

$\sigma = dI/dV(V)$

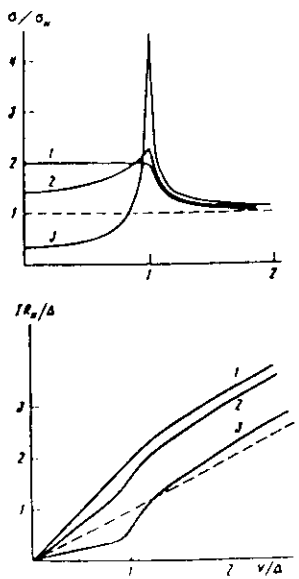

clean contact

$d << l$

$d << \xi_0$

T=0

$Z_1=0; \quad Z_1<Z_2<Z_3$

Zaitsev, JETP **51**, 111 (1980)
Blonder, Tinkham, Klapwijk, (BTK
PR **25**, 4515 (1982)
Zaitsev, JETP **59**, 1015 (1984)

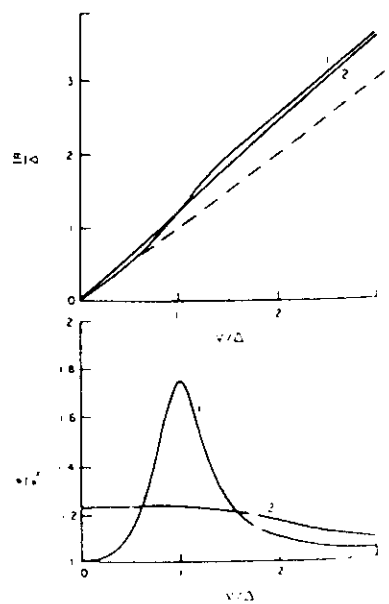

dirty contact

$d >> l$

$d << (\xi_0 l)^{1/2}$

1 - $T/\Delta=0.1$
2 - $T/\Delta=0.7$

Artemenko, Volkov, Zaitsev (AVZ)
SSC **30**, 771 (1979)

andrtheo org

Fig.9

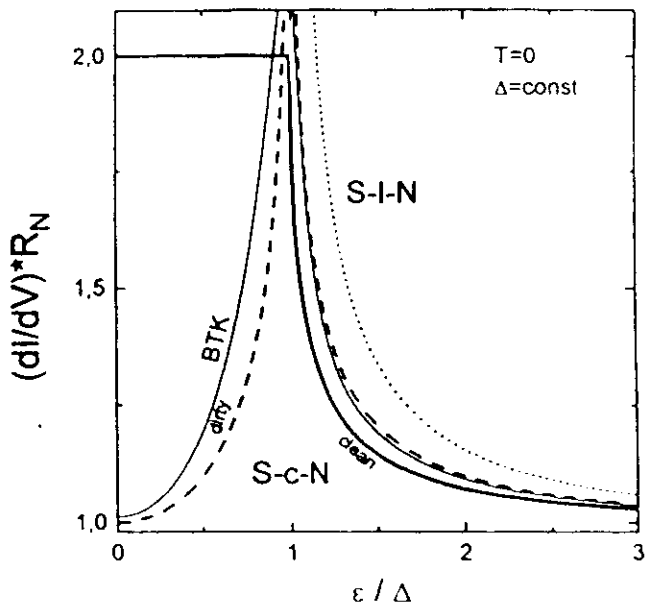

Fig.10

A parallel study of the excess current in the superconducting state and the electron-phonon interaction function in the normal state

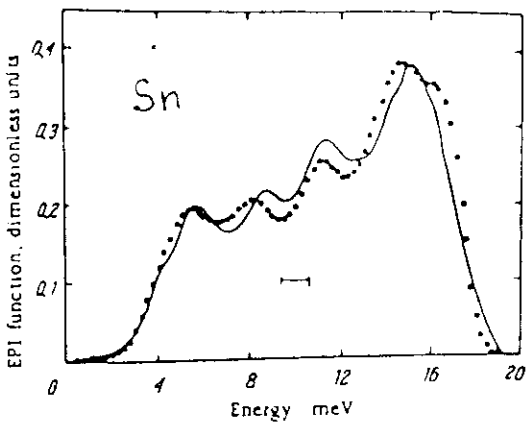

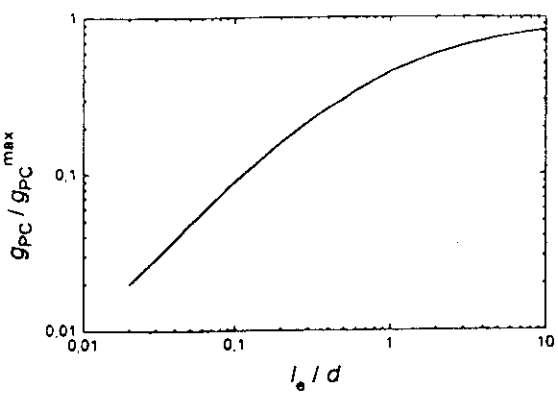

Fig.11

A parallel study of the excess current in the superconducting state and the electron-phonon interaction function in the normal state

$$\delta I_{N(S)} = I_{N(S)}(V) - V/R_0$$

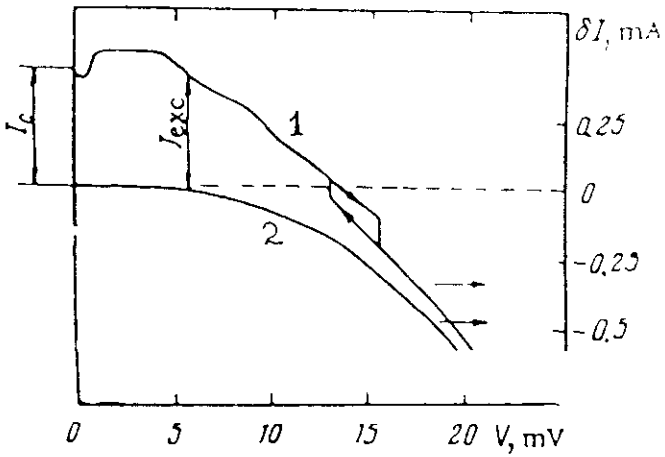

Excess current:

Dirty limit: $I_{exc} = [(\pi^2/4) - 1](\Delta/eR_0) = 1.47(\Delta/eR_0)$;

Clean limit: $I_{exc} = (8/3)(\Delta/eR_0) = 2.67(\Delta/eR_0)$;

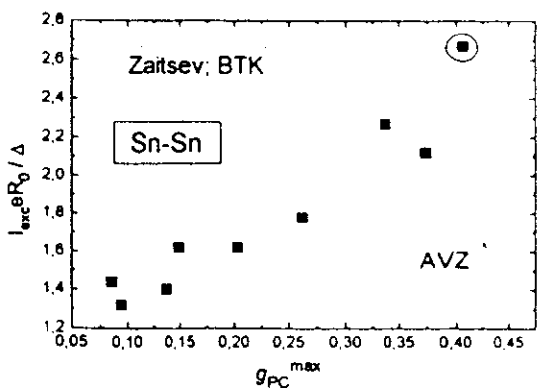

Khotkevich, Yanson, Sov. J. Low Temp. Phys. 7, 354 (1981)

Fig.12

Electron-phonon interaction effects on excess current

$$I_{exc}(eV >> \Delta) \neq const$$

$dI/I_{in} < 1$

$\Delta = \Delta(\varepsilon)$

$$I(V) = V/R - \delta I_{ph}^{N}(V) + I_{exc}(V); \qquad I_{exc}(V) = I^{(0)}_{exc} - \delta I^{S}_{ph}(V)$$

$\sim I(V)(dI/I_{in})$

$$\delta I^{S}_{ph}(V) = \delta I^{S}_{in}(V) + \delta I^{S}_{el}(V)$$

$\sim I^{(0)}_{exc}(dI/I_{in})$ $\qquad$ $\sim I^{(0)}_{exc}(\Delta(\varepsilon)/\hbar\omega_{ph})$

Inelastic scattering via Andreev reflection: S-c-N junction. Theory.

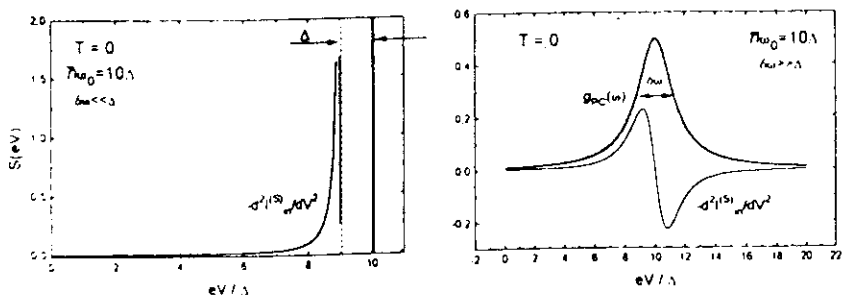

$$\frac{1}{R}\frac{dR}{dV} = \frac{4ed}{3\pi}\sum_{\alpha=1,2}\frac{1}{v_F^{(\alpha)}}\int_0^\infty \frac{d\omega}{\Delta} S\left(\frac{\omega - eV}{\Delta}\right) g_{PC}^{(\alpha)}(\omega) \qquad \text{for } T \ll \Delta.$$

$$R = \frac{dV}{dI}, \qquad S(x) = \theta(x \quad 1)\frac{2(x - \sqrt{x^2 - 1})^2}{\sqrt{x^2 - 1}}.$$

For $\hbar\omega \gg \max(\Delta, T)$, $\qquad \frac{1}{R(V)} - \left(\frac{1}{R(V)}\right)_{\Delta \to 0} = \frac{8}{3R}\frac{d\Delta}{\hbar}\sum_{\alpha=1,2}\frac{1}{v_F^{(\alpha)}} g_{PC}^{(\alpha)}(eV)$

Khlus, Omel'yanchuk, SJLTP 9, 189 1983)
V. Khlus, SJLTP 9, 510 (1983)

Fig.13

el-phe1a.org

Inelastic scattering via Andreev reflection

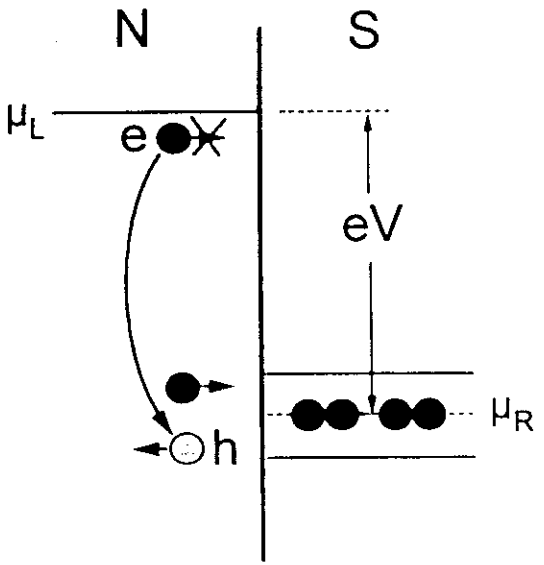

$g_{PC}(\omega) \sim \delta(\omega - \omega_0)$

$\delta I_{in}^{(A)} \neq 0$ for $|eV| < \hbar\omega_0$

$d^2I/dV^2 = 0$ for $\hbar\omega_0 - \Delta < |eV| < \hbar\omega_0$;

$d^2I/dV^2 \neq 0$ for $|eV| < \hbar\omega_0 - \Delta$.

Fig.14

khlus1.org

Inelastic scattering via Andreev reflection. Experiment.

Yanson *et al*., SJLTP 10, 221 (1984)

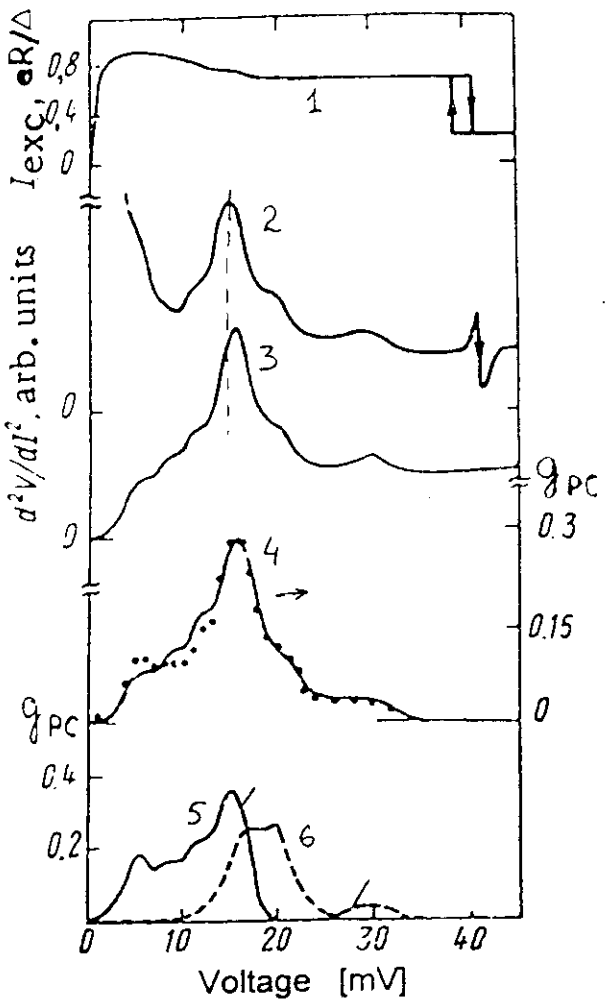

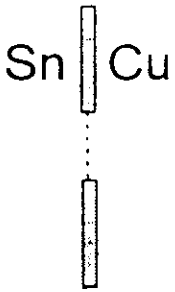

$d < \xi_0$

$d < l_{in}, l_e$

$\hbar\omega_{ph} >> \Delta_0$

ξ_0=270 nm
d=10 nm
R_0=8.8 Ω

$$g_{PC}(\text{Sn-Cu}) \cong (1/2)[g_{PC}(\text{Sn}) + g_{PC}(\text{Cu})]$$

Fig.15

Elastic contribution to the nonlinearity of S-c-N junction

Omel'yanchuk *et al*, SJLTP 14 630 (1988)

normal - inelastic: d / l_i ;

super - elastic: $(\Delta / \hbar\omega_{ph})^2$;

excess - inelastic: $(d / l_i)(\Delta / \hbar\omega_{ph})$

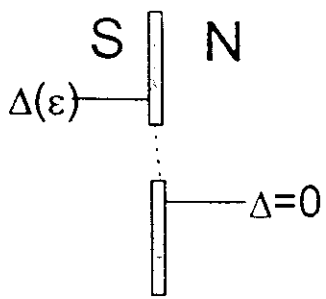

$d << \xi_0$

$$\left\{\frac{dI}{dV}(eV)\right\}_{S-c-N} = \frac{1}{R_0}\left\{1 + \left|\frac{\Delta(\varepsilon)}{\varepsilon + \left[\varepsilon^2 - \Delta^2(\varepsilon)\right]^{1/2}}\right|^2\right\}_{\varepsilon = eV}$$

Compare with Rowell-McMillan-Dynes expression

$$\left\{\frac{dI}{dV}(eV)\right\}_{S-I-N} = \frac{1}{R_0}\,\mathrm{Re}\left\{\frac{\varepsilon}{\sqrt{\varepsilon^2 - \Delta^2}}\right\}_{\varepsilon = eV}$$

Experiment: Khotkevich *et al*, SJLTP 16, 693 (1990)

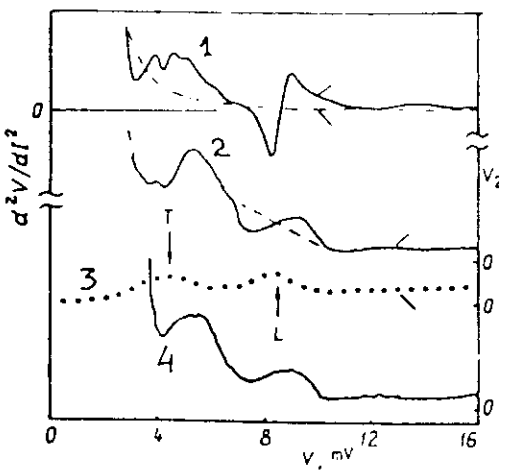

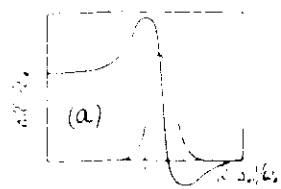

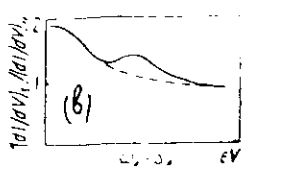

Pb - Ru [1010]
Pb - Os [1010]

T=1.7 K

Fig.16

Phonon singularities on volt-ampere curves of *dirty* S-c-S contacts

(Experiment)

Yanson *et al*, SSC **60**, 515 (1984)

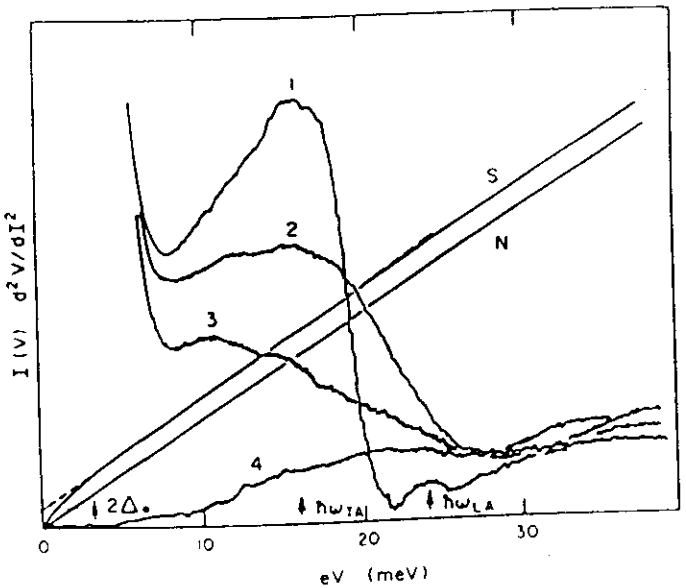

Nb - Nb

R_0=30 Ω

1 - 4.4 K
2 - 6.5 K
3 - 8.65 K
4 - 10.8 K

S - 7.8 K
N - 11.2 K

$R_0 I_{exc}$=1.9 mV (exp.)
$R_0 I_{exc}$=2.2 mV (theor.)

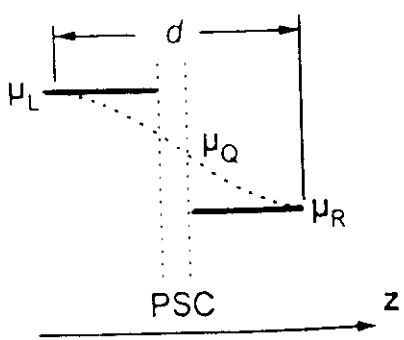

d ~ 5 nm
ξ_0 ~ 40 nm
$l_{in}(\omega_{max})$ ~ 6 nm

$\xi_0 > d \sim l_{in}$

$\xi > d \sim \Lambda_{in}$

For clean contact $\left(\frac{dI_{exc}}{dt}\right)_{clean} = \frac{-1}{l_{in}} \frac{16}{3\pi} \left(\frac{d}{\xi_0}\right) \left[q^N(eV) + q^N(eV)\right]$, $(\delta_{in} \gg \Delta)$

In normal state $g^N_{PC,dirty} \sim \left(\frac{l_i}{d}\right) g^N_{PC,clean}$

Fig.17

el-phex3.org

Change of the order of phase transition in a superconductor under the contact

Naidyuk *et al*, PR B **64**, 16077 (199

Zn - Ag

Zn_{bulk}: T_c=0.875 K; B_c=5.3 mT; ξ_0=2000 nm; λ_L=30 n

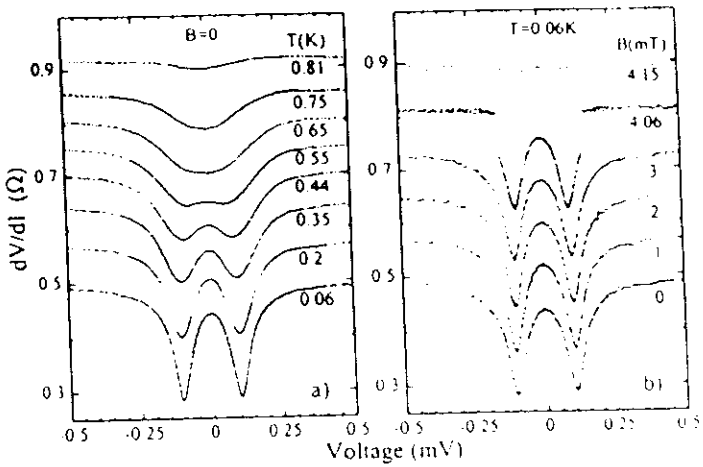

R_N=0.5 Ω
T_c=0.82 K
B_c=4.1 mT

BTK-fit:
T=0.06 K
B=0
Δ=110 μeV
Γ=6 μeV
Z=0.5

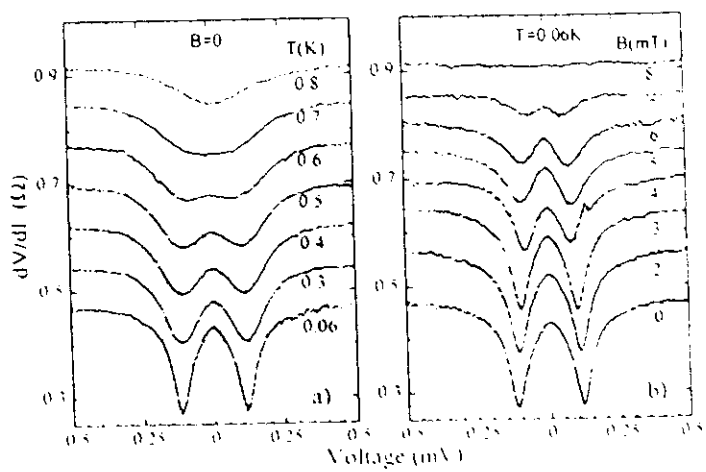

R_N=0.47
T_c=0.83
B_c=8 mT

BTK-fit:
T=0.06 K
B=0
Δ=124 μ
Γ=6.5 μ
Z=0.51

$Z_{BTK}(v_F)=(1-r) / 2r^{1/2}=0.13$; $r=v_{F1}/v_{F2}$

Fig.18

naid_1.o

Influence of magnetic field: $\Gamma(B)$, $\Gamma(d)$

Zn - Ag

type - I type - II

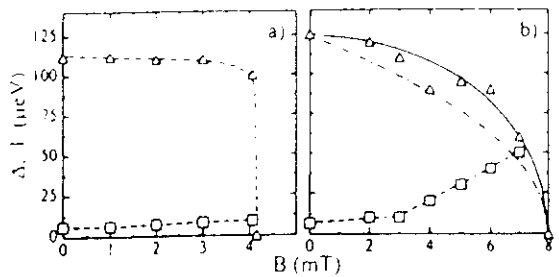

B_{c2} dirty --> $l \sim \Phi_0/2\pi\xi_0 B_{c2}$ --> $\xi \sim (\xi_0 l)^{1/2}$ --> $\lambda \sim \lambda_L(\xi_0/l)^{1/2}$;

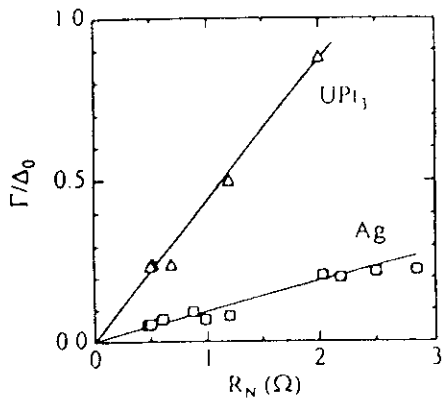

d --> $R_N \sim \rho/d + 16\rho l/3\pi d^2$

Fig.19

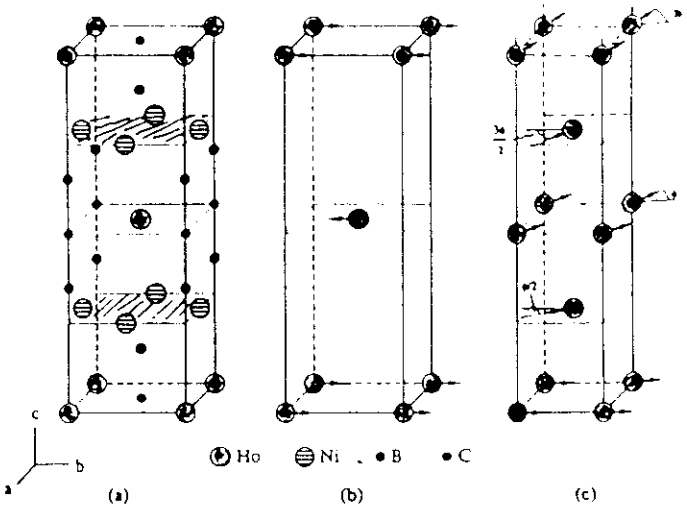

FIG. 1. $HoNi_2B_2C$ (a) crystal structure; (b) commensurate antiferromagnetic structure; (c) spiral magnetic structure.

Fig.20

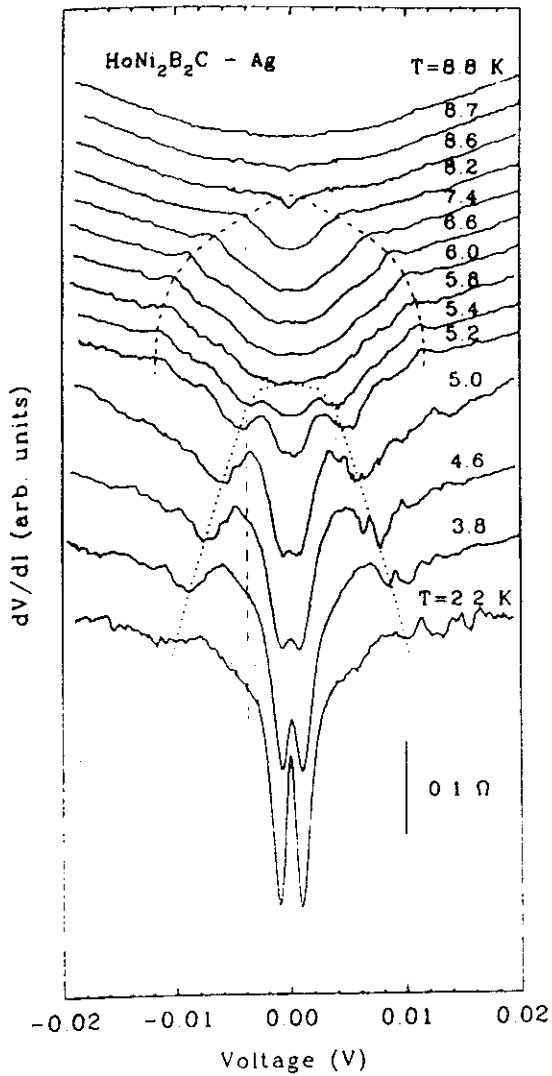

Fig.21

Excess current in case of strong unpairing

Rybaltchenko *et al*, Europhys. Lett. 33,483 (19

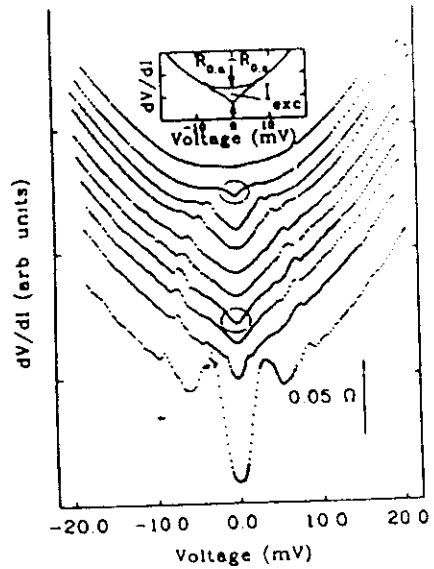

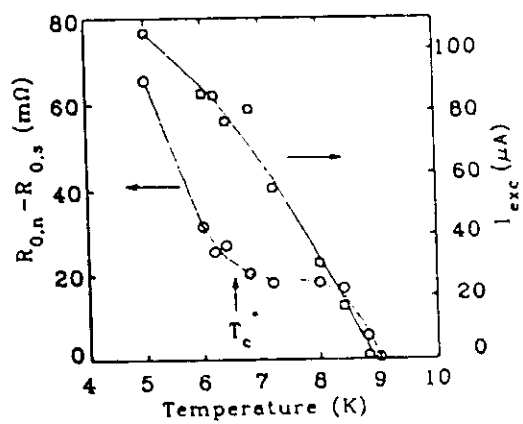

Beloborod'ko, Omel'yanchuk, SJLTP, 17,516

For strong unpairing: $I_{exc}=(\pi^3/4eR)\,(T_c^2/\Gamma)\,\tanh(eV/2T)\,(1-T^2/T_c^2)$

$T \to T_c$: $I_{exc} \sim (1-T/T_c)$,

while for $\Gamma=0$: $I_{exc} \sim \Delta_0(t) \sim (1-T/T_{c0})^{1/2}$

Fig.22

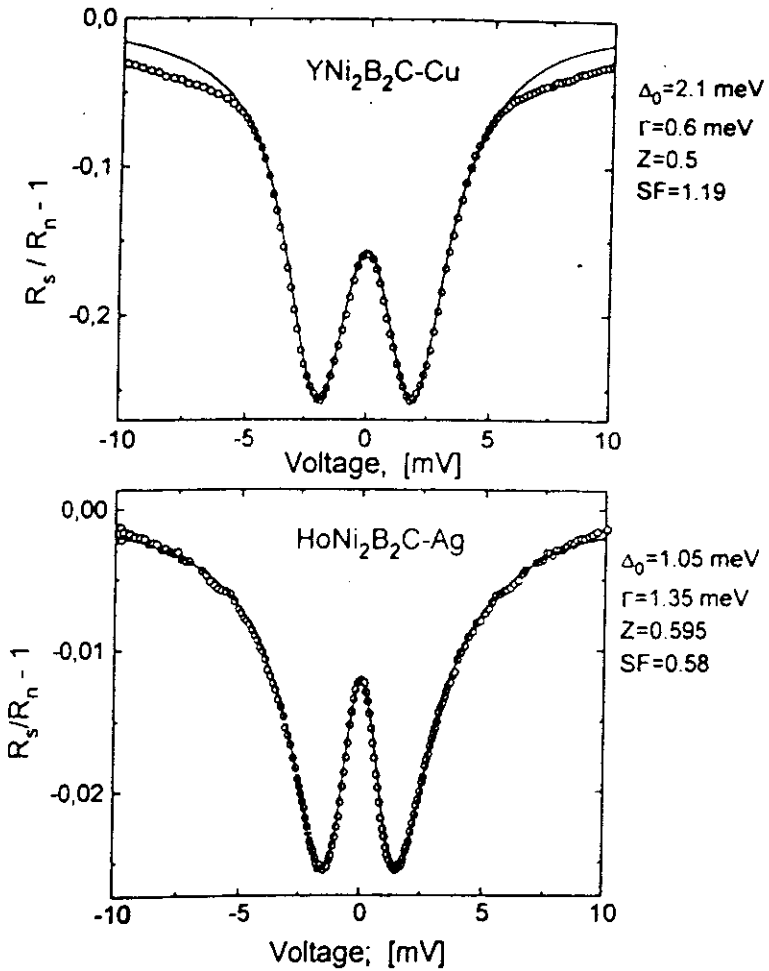
YNi2B2C-Cu
Δ0=2.1 meV
Γ=0.6 meV
Z=0.5
SF=1.19
Rs / Rn - 1
Voltage, [mV]
HoNi2B2C-Ag
Δ0=1.05 meV
Γ=1.35 meV
Z=0.595
SF=0.58
Rs/Rn - 1
Voltage; [mV]

Fig.23

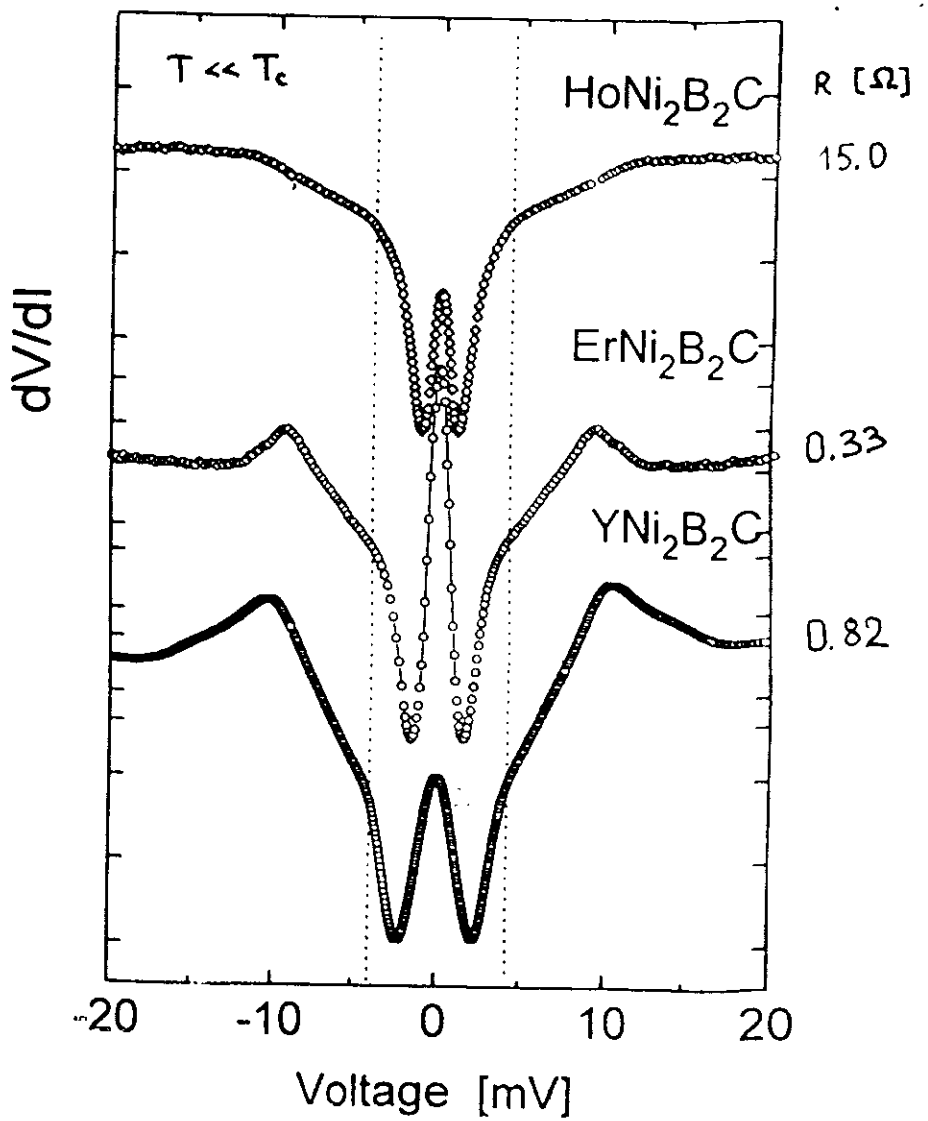
T << Tc
HoNi2B2C
ErNi2B2C
YNi2B2C
R [Ω]
15.0
0.33
0.82
dV/dI
Voltage [mV]

Fig.24

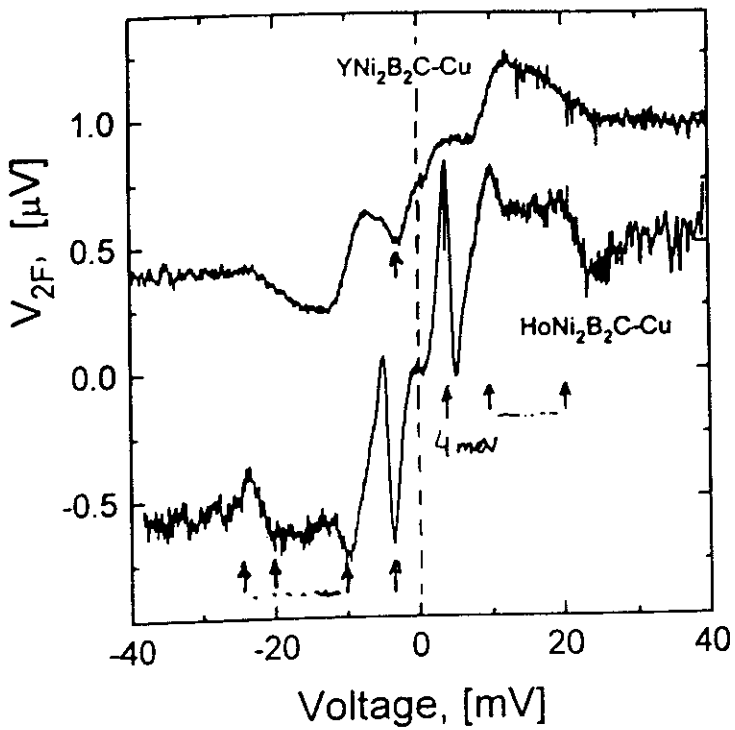

eV_{ph} : 4 meV ; 9.4 ... 15 ... 19.4 meV

Fig.25

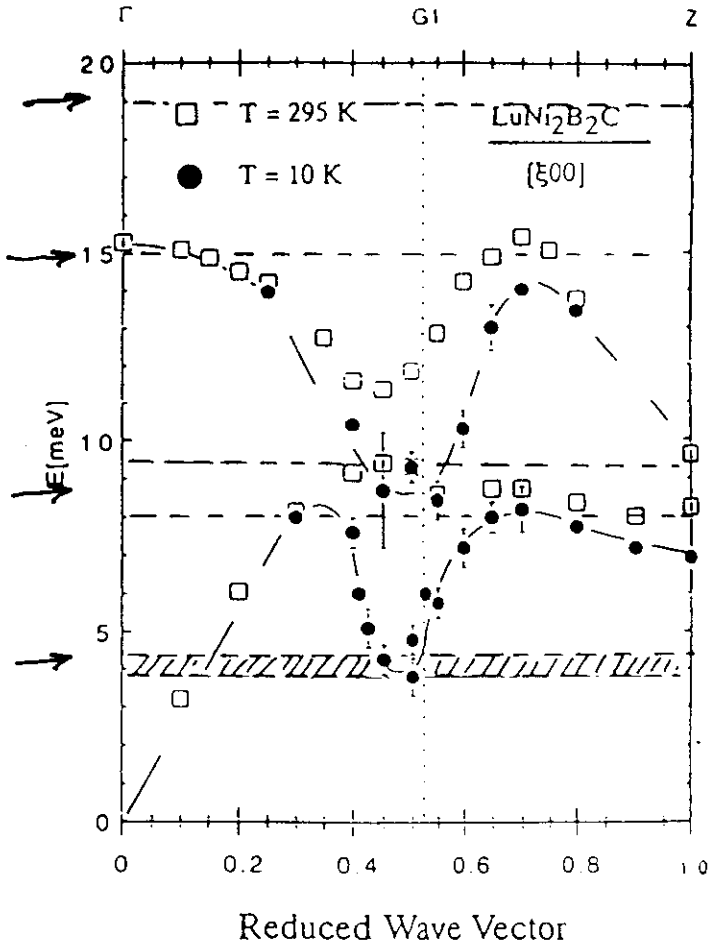

FIG. 2. The Δ_4 [ξ00] branches at 295 and 10 K. The lines through the 10 K points are intended as guides to the eye.

Fig.26